Scientia Iranica A (2019) 26(1), 202–212

Sharif University of Technology
Scientia Iranica
Transactions A: Civil Engineering
http://scientiairanica.sharif.edu

Antecedent rainfall induced shallow landslide: A case study of Yunnan landslide, China

Z. Li[a,b,*], Y.J. He[a,b], H. Li[a,b], L.J. Wang[c], and Y.Q. Wang[d]

a. *Dam Safety Management Department, Nanjing Hydraulic Research Institute, Guangzhou Road 225, Nanjing 210029, China.*
b. *Dam Safety Management Center of the Ministry of Water Resources, Guangzhou Road 225, Nanjing 210029, China.*
c. *College of Water Conservancy and Hydropower Engineering, Hohai University, Xikang Road 1, Nanjing 210098, China.*
d. *School of Civil Engineering, Hefei University of Technology, Tun-Xi Road 193, Hefei 230009, China.*

Received 17 January 2017; received in revised form 10 May 2017; accepted 12 June 2017

KEYWORDS
Antecedent rainfall;
Landslide;
Numerical modeling;
Slope stability;
Unsaturated soil.

Abstract. We present a case study of antecedent rainfall induced failure of engineering slope. The impacts of pore-water pressure, pore-water pressure increment, water content, and the factor of safety are investigated by numerical models for an actual slope in Yunnan, China. The results indicate that antecedent rainfall plays an important role in the stability of the slope. The model reasonably explains the time lag between the occurrences of rainfall and landslides. Pore-water pressures significantly change at the upper layer of red-clay slope; the occurrence of cracks at the top of the slope agrees with the field observations before landslide. The saturated zone of the slope gradually expands from the top to bottom of the slope; the major reason for landslide is that the surface stagnant water, after rainfall, gradually infiltrates into the weathered gneiss rock, resulting in decrease in the strength of weathered gneiss rock. Then, the weight of the later rainfall leads to landslide of the slope. The factor of safety of the slope is evaluated by the modified limit equilibrium methods. It is shown that the actual failure occurs when the calculated factor of safety approaches its minimum, i.e., 0.97. The landslide is characterized by shallow landslides.

1. Introduction

Landslides are disastrous physical and geological phenomena, which have various scales and complex mechanisms, and frequently occur due to extreme climate effects. It is a special natural hazard, which is like rock fall and debris flow. A number of studies have indicated that the slope failures can be attributed to several factors such as climate conditions, geological features, topography, rainfall, earthquake, reservoir water level, vegetation, and soil spatial variability, either separately or together [1-3]. Rainfall has a direct effect on occurrence of landslides. It is widely recognized that rainfall-induced slope failures are mainly caused by infiltration of rainwater [4-6]. The role of rainfall infiltration in triggering landslides in tropical regions has been a challenging issue for geotechnical engineers and engineering geologists. Rainfall-induced shallow landslides affecting superficial deposits of small thickness (generally lower than 2 m) are common phenomena all over the world.

Early studies of rainfall and landsliding in Hong Kong [7] utilized only the rainfall data at one location for correlations with landsliding across the entire Territory of Hong Kong. Rainfall of 1-12 h duration is important in predicting the number of landslides; antecedent rainfall also has some influence [8]. There have been different conclusions as to the relative roles of

*. *Corresponding author. Tel.: +86 25 85828141; Fax:+86 25 83714644*
E-mail address: slxliz@163.com (Z. Li).

doi: 10.24200/sci.2017.4234

antecedent rainfall in landslides. Brand concluded that antecedent rainfall was not a major factor, except in the case of minor landslide events (i.e., only a small number of landslides) occurring under relatively low intensity rainfalls [9]. Brand concluded that the majority of landslides were caused by localized, short-duration, high-intensity rainfalls, and that a large proportion of the landslides took place in severe rainstorms as the peak of hourly rainfall and a smaller proportion occurred sometime afterwards [9]. Tan suggested that the antecedent rainfall could be significant in affecting the slope stability [10]. Wei in a case study of the Bukit Batok landslides in Singapore found that the failure occurred after a period of heavy rainfall and there was no rainfall at the time of failure [11]. Antecedent rainfall, initial pore-water pressures prior to a significant rainfall event, and the magnitude of the rainfall event play a crucial role in the development of the worst pore-water pressure condition in a slope [12].

Soil water content, pore water pressure, and matric suction are the basic soil features to be considered in the stability analysis of the slope during a rainfall event. Soil water content, pore water pressure, and matric suction data from continuous monitoring of unsaturated soils have been proved very useful in different kinds of stability models, such as closed-form equations based on a limit equilibrium analysis [13-15], physically based models [16-19], and Finite Element Models (FEM).

Many authors identified the quick increase in pore water pressure and the development of positive pore pressures, due to the formation of a perched water table, as the most important causes for shallow landslide triggering [5,20-23]. It is generally recognized that rainfall-induced landslides are caused by changes in pore-water pressures. The increase in pore pressure decreases soil effective stress and, thus, reduces soil shear strength.

Numerical models have been used for simulating the mechanism of rainfall-induced slope failure. Many authors studied the effect of rainfall infiltration in a typical unsaturated hillside, e.g., Ng and Shi, who used a steep cut slope in Hong Kong in their study [24]. Limit equilibrium methods are most widely used for analyzing the slope stability and designing engineered slopes. Finite element program Seep/W was employed to compute the pore-water pressures, which were required for the calculation of safety by conventional limit equilibrium method. Tsaparas performed a numerical simulation to investigate the responses of a typical residual soil slope in Singapore to several hydrological parameters including rainfall distribution, saturated permeability of soil, initial pore-water pressures, and groundwater table [25]. Over the previous century, a variety of limit equilibrium techniques have been developed to determine stability conditions, depending on the equations of equilibrium included and the assumptions made to account for the inter-slice forces [26-29].

The key indicator in slope stability analysis is the Factor Of Safety (FOS), which is commonly defined as the ratio of the resisting shear force to the driving shear force along a failure surface [30-32].

The main objectives of the present work can be summarized as follows:

1. To study a case where antecedent rainfall and landslides occurred in Yunnan province of china on August 17, 2013;
2. To analyze pore-water pressure, pore-water pressure increment, water content, and the factor of safety in the change of the slope by antecedent rainfall;
3. To present a systematic methodology to explain the mechanism of rainfall-induced landslide in unsaturated slopes.

2. Landslide description

2.1. Site description

The selected study site shown in Figure 1 is located

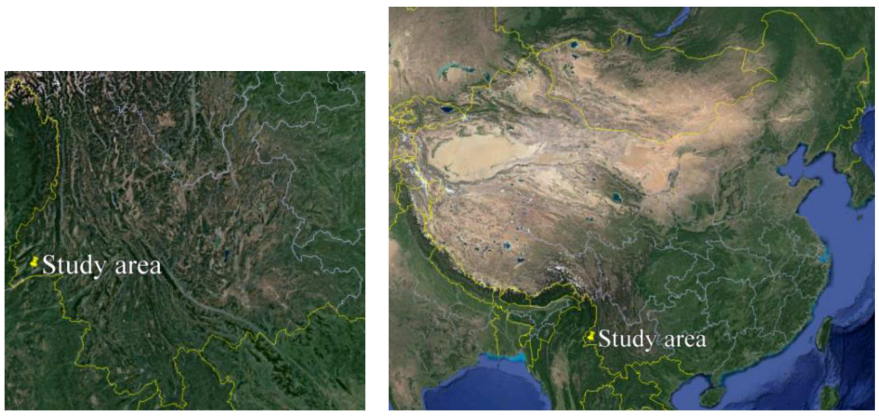

Figure 1. Location map of the study area with distributions of landslide dam in China.

in the west of Yunnan in China (24°14′N and 98° 06′E). The study area has a South Asian tropical humid climate zone, with a hot rainy weather in summer and autumn, and a mild and relatively dry winter. The mean annual temperature is high, above 20°C, with mean daily summer temperature ranging from 29° to 35° and a maximum temperature of 35.7°C in mid-August and a minimum temperature of 11.2°C in the late January. The annual rainfall period is 180 days, rainy season from May to October every year, which accounts for 82% of the rainfall in a year. Multi-year average precipitation of the study area is 1709 mm. The area is located about 70 km away from Mangshi City at an elevation of 2000 m. On 17th August 2013, landslide occurred in the area at the end of 4 days of high-intensity rainfall.

On August 17, 2013, at 6:00 AM, 40000 m^3 of soil failed over a deep surface (Figures 2 and 3). From the field observations, the height of landslide was roughly estimated to be 100 m, while the width of the slide varied from 21 m to 63 m and the depth of the slide varied from 5 m to 13 m, with the mean slope angle varying from 45°to 50°. The area affected by landslide was 40000 m^2 and the event of the slide from crown to toe measured 100 m. The failure caused structural damages to an adjacent building and an electrical control room of the dam, and interrupted the traffic. Luckily, the slide did not cause any loss of life. On the following day, there were indications of groundwater springs at the upper region.

Daily pluviometric records, provided by the Longjiang monitoring station, are presented in Figure 4. The accumulated rain amount from August 1 to August 23 (23 days) summed a total of 250.1 mm. The slope failure occurred when the rain had already ceased. The accumulated rain amount was 30.6 mm from January 2011 to August 2013, which led to continuous drought in the study area. Preliminary analyses indicated that the slope instability could have been caused by the rise of the water table due to rainfall infiltration.

2.2. Geological setting of the slope

The geology of the study site is briefly described. Also, simplified geological map of the site is shown in Figure 3. Geologically, the slope was composed of red clay originating from strong weathering gneiss. Red clay was characterized by the dispersion of soil structure, which was mainly distributed in the middle and the top of the slope; the overlying red clay indicated depths varying from 6 to 8 m. Strong weathered gneiss rock was composed of feldspar, quartz, and biotite, which were characterized by macroscopic cataclastic and microscopic mylonitic structures. The transition between the strong weathered gneiss rock and red clay was weathered gneiss rock, which was composed of

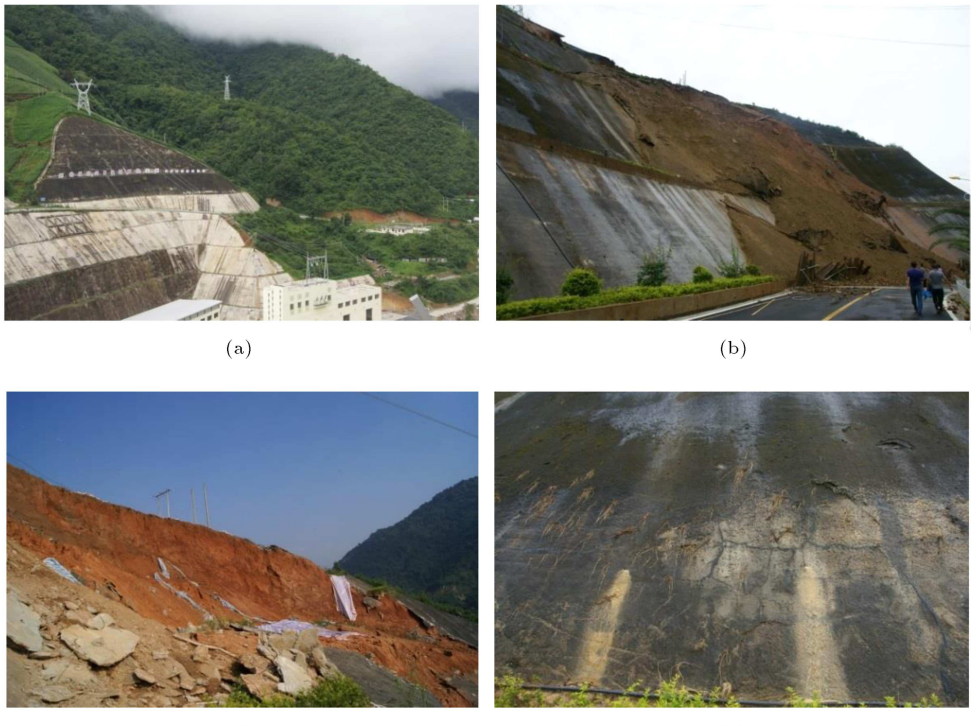

Figure 2. Landslide triggered by the August 17, 2013 antecedent rainfall event in the western Yunnan in China: (a) Before the landslide, (b) landslide body, (c) the rear of landslide body, and (d) the landslide body of groundwater level.

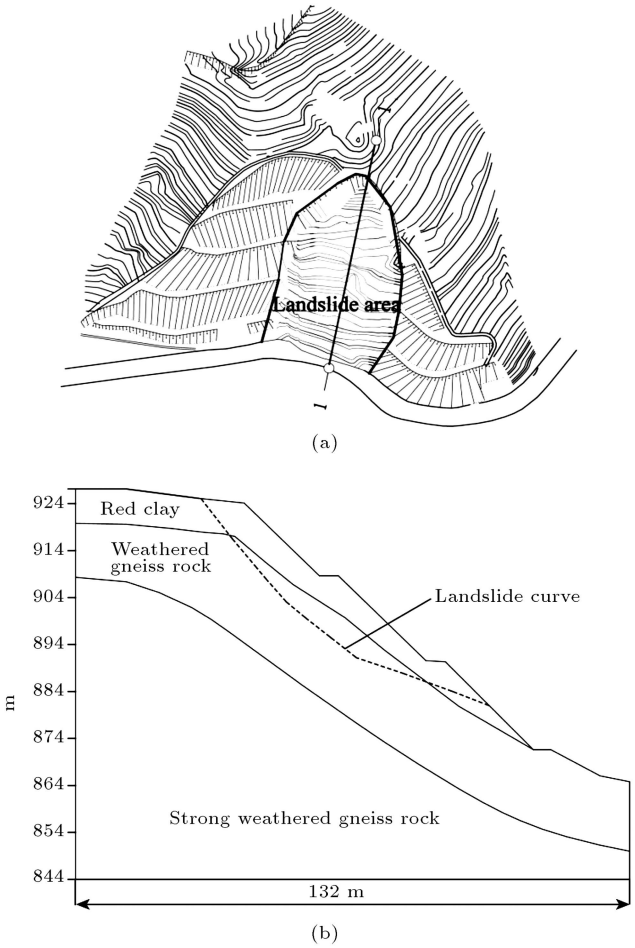

Figure 3. Simplified geological map and landslide inventory map of the study area: (a) Schematic site plan before landslide and (b) soil profiles of the slope (profile 1-1).

feldspar, quartz, and biotite with the thickness varying from 15 to 20 m.

3. Numerical modeling

3.1. Flow model

The general flow equation that controls steady-unsteady state flow problem through a 2-D saturated-unsaturated porous medium, usually referred to as Richards equation, can be written as:

$$\frac{\partial}{\partial x_i}\left[k_{ij}^s k_r(h_c)\frac{\partial h_c}{\partial x_j} + k_{i2}^s k_r(h_c)\right] - Q = [C(h_c) + \beta S_s]\frac{\partial h_c}{\partial t}, \quad (1)$$

where, h_c is the pressure head; θ is the volumetric water content; k_{ij}^s is the hydraulic conductivity tensor at saturation; k_r is the relative hydraulic conductivity, which is defined as the relationship between unsaturated and saturated hydraulic conductivities (k/k_{sat}); k_r varies between 0 and 1 and is a scalar function of the degree of saturation; $C(\varphi)$ is the volumetric water retention capacity $\partial\theta/\partial h_c$; S_s is the specific storage coefficient; and Q is the source sink term.

The calculation of Soil-Water Content Characteristic (SWCC) curve has been proposed by Van-Genuchten:

$$S_e = \left[1 + (s/P_0)^n\right]^{-m}, \quad (2)$$

$$m = 1 - \frac{1}{n}, \quad (3)$$

where s is the matric suction ($u_a - u_w$); p_0 is air entry value; n and m are the curve fitting parameters, respectively; and S_e is the effective water saturation. According to Van-Genuchten, hydraulic conductivity of soil changes by:

$$k_{rl} = \begin{cases} S_e^{1/2}\left[1 - (1 - S_e^{1/m})^m\right]^2 & S_w < S_{sw} \\ 1 & S_w \geq S_{sw} \end{cases} \quad (4)$$

$$k = k_{rl}k_{sat}, \quad (5)$$

where k_{rl} is the relative hydraulic conductivity; k_{sat} is the saturated hydraulic conductivity (m/s); S_{sw} is the maximum saturation of soil; and S_e is the effective water saturation.

3.2. Geometry and boundary conditions

The slope weathering profile was composed of an averagely 2 m thick superficial mature residual soil.

The lateral boundaries were considered as impervious surfaces. This implies that flow directions were parallel to the boundaries of the slope. The bottom of the slope was considered as an impervious surface. These boundary conditions are favorable to the development of positive pore pressure. At the slope surface, daily rainfall events were simulated by prescribing flow velocities computed according to daily rain amount registered at the study area. The rainfall was relatively low, due to the occurrence of drought from 2010 to 2012 in the study area; thus, water table was low. In order to make the initial water table consistent with the actual situation, average rainfall of years was used as the initial condition of infiltration (Figures 4-6). Groundwater recharge was mainly supplied by rainfall.

3.3. Hydraulic parameters

The parameters are presented in Table 1. Red clay, weathered gneiss rock, and strong weathered parameters were obtained by laboratory experiment.

3.4. Strength of unsaturated soil

In this study, the extended Mohr-Coulomb shear strength equation [33] is adopted in the 2-D general limit equilibrium method:

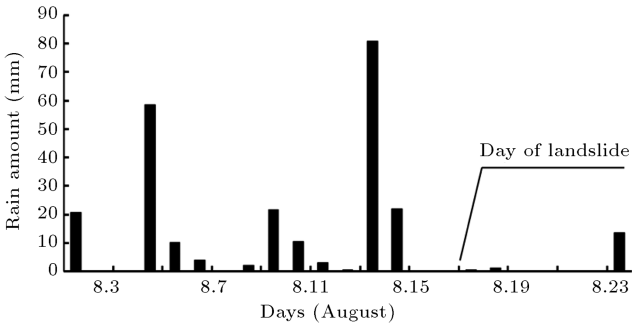

Figure 4. Daily rain amount.

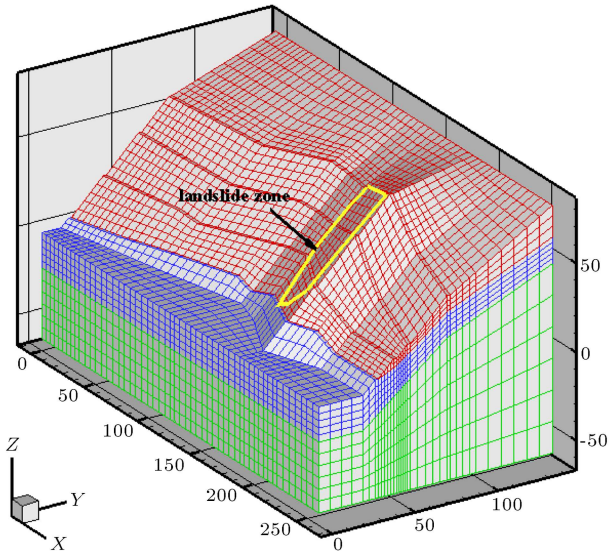

Figure 5. 2-D finite element meshes.

$$\tau_f = c' + (\sigma - u_a)\tan\varphi' + (u_a - u_w)\tan\varphi^b, \qquad (6)$$

where c' is the effective cohesion; τ_f is the shear strength; $(\sigma - u_a)$ is the net normal stress on the failure plane, in which σ is total normal stress and u_a is the pore-air pressure; $(u_a - u_w)$ is the matric suction, in which u_w is the pore-water pressure; and φ^b is the rate of increase in shear strength relative to the matric suction.

3.5. Unsaturated soil slope stability analysis method

Two-Dimensional (2-D) Limit Equilibrium Methods (LEMs) of slope stability analysis are the most common ones in slope engineering. On the basis of simplified Bishop method, combined with the finite element method and the stability analysis method, which simulate negative pore water pressure and matric suction of soil, the safety factor is obtained under the condition of rainfall infiltration of the slope. The method is presented in Figure 7.

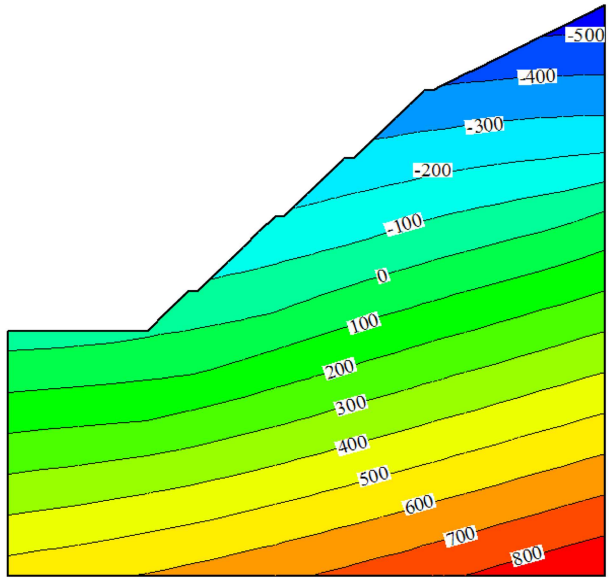

Figure 6. The initial water head contour.

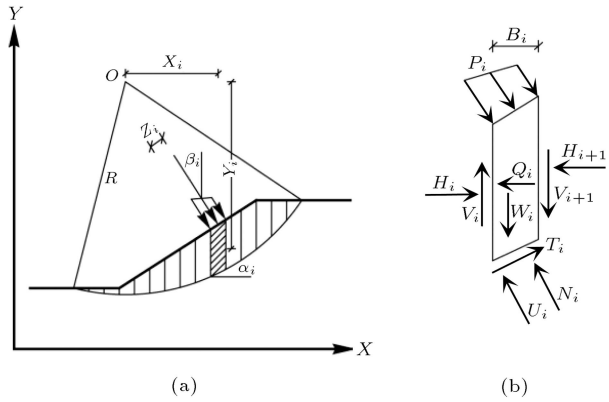

Figure 7. Free body diagram of the two-dimensional general limit equilibrium method.

The factor of safety with respect to moment equi-

Table 1. Parameters of modeling.

Material	G_s	e	S_{sw} (%)	S_r (%)	p_0 (kPa)	n	k_{sat} (m/s)
Red clay	2.80	0.92	77	45	20	1.16	1.69e-3
Weathered gneiss rock	2.85	0.83	85	45	10	1.13	5.0e-3
Strong weathered gneiss rock	–	–	–	–	–	–	2.0e-4

Note: G_s = specific gravity of rains; e = voids ratio; n =porosity; S_{sw} = the maximum saturation of soil; p_0 = air entry value; k_{sat} = the saturated hydraulic conductivity.

$$FOS = \frac{\sum \frac{1}{m_i} \left\{ [c'_i + (u_a - u_w) \tan \varphi^b] L_i \cos \alpha_i + (W_i + P_i \cos \beta_i - U_i \cos \alpha_i) \tan \phi'_i \right\}}{\sum W_i \frac{X_i}{R} + \sum Q_i \frac{Y_i}{R} + \sum P_i \frac{Z_i}{R}}. \quad (7)$$

Box I

librium, F_m, by considering the effect of matric suction is calculated by Eq. (7) as shown in Box I, where c'_i is the effective cohesion; w_i is weight; Q_i is horizontal earthquake force; H_i and H_{i+1} are normal forces; V_i and V_{i+1} are tangential forces; N_i is effective force; U_i is pore-water pressure; T_i is tangential shearing resistance; P_i is linear distributed load; and R is the sliding arc radius of the slope.

3.6. Strength parameters

The parameters are presented in Table 2. They were obtained by experiments. The strength of red clay and weathered gneiss rock decreased obviously after rainfall saturated, which was mainly due to reduced suction. Natural water content and saturated water content of matric suction according to Soil-Water Content Characteristic (SWCC) curve, red clay parameters, and weathered gneiss rock parameters were obtained by Mohr-Coulomb shear strength equation [33] . Red clay parameters and weathered gneiss rock are shown in Table 3.

Table 3. Unsaturated soil parameters.

Materials	Red clay	Weathered gneiss rock
φ' (deg)	17.3	23
c' (kPa)	23.9	18
φ^b (deg)	12.4	20

4. Results

4.1. Influence of pore-water pressure and water content

Previous study results have demonstrated that the stability of the slope is directly related to rainfall. Antecedent rainfall and landslides in Yunnan province of China were characterized by shallow sliding, and sliding surface between red clay and weathered gneiss rock; thus, pore-water pressure, pore-water pressure increment, and the various characteristics of water content of red clay and weathered gneiss rock were analyzed in the study, respectively.

Figure 8 illustrates the variations of pore-water

Table 2. Strength of parameters.

Materials		Red clay	Weathered gneiss rock	Strong weathered gneiss rock
γ (kN/m^3)		17.3	18.2	22.6
γ_{sat} (kN/m^3)		17.8	18.8	23.0
Natural soils	φ (deg)	17.0	23.0	28.0
	c (kPa)	45.0	47.0	50.0
Saturated soil	φ (deg)	16.0	18.0	28.0
	c (kPa)	22.0	30.0	45.0

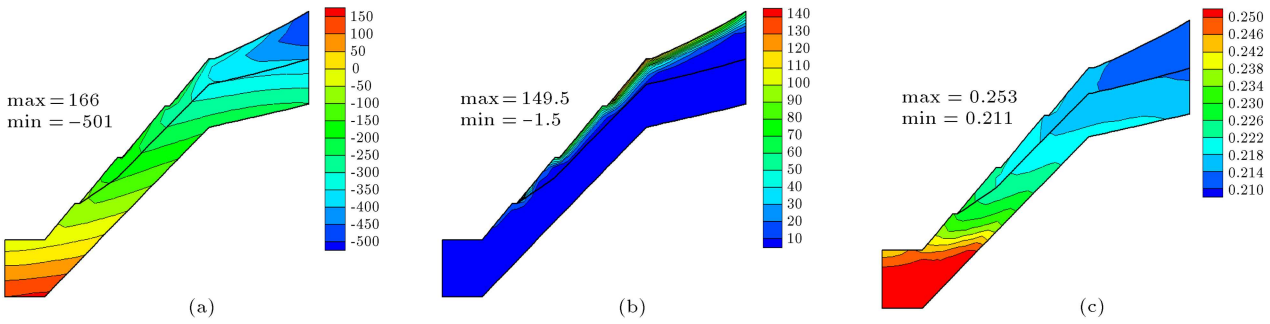

Figure 8. Simulated results at the study site: (a) Pore-water pressure (kPa) on August 1, 2013, (b) the increment of pore-water pressure (kPa) on August 1, 2013, and (c) water content on August 1, 2013.

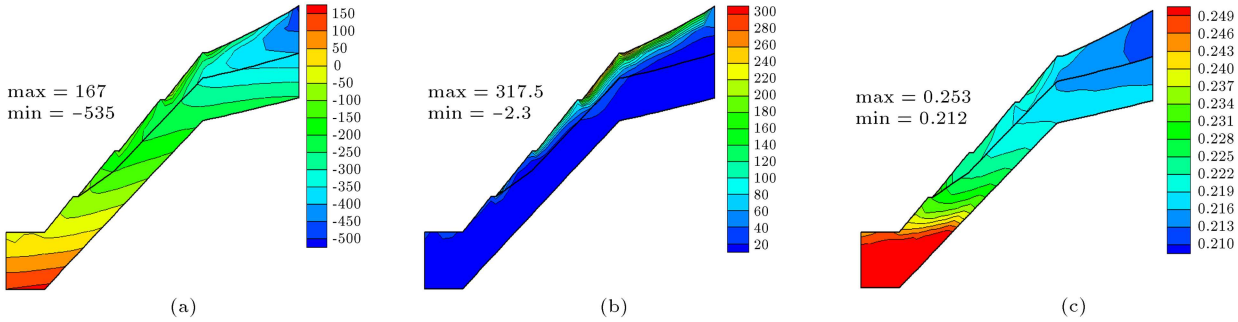

Figure 9. Simulated results at the study site: (a) Pore-water pressure (kPa) on August 4, 2013, (b) the increment of pore-water pressure (kPa) on August 4, 2013, and (c) water content on August 4, 2013.

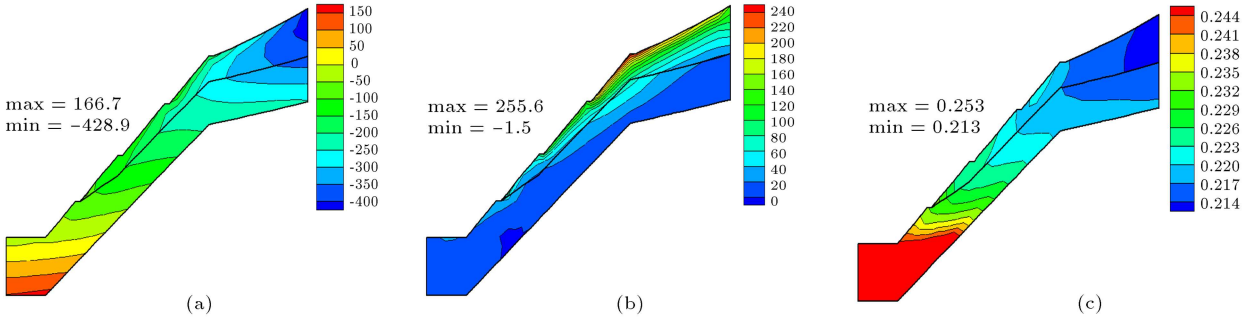

Figure 10. Simulated results at the study site: (a) Pore-water pressure (kPa) on August 9, 2013, (b) the increment of pore-water pressure (kPa) on August 9, 2013, and (c) water content on August 9, 2013.

pressure, pore-water pressure increment, and water content characteristics of the slope on August 1, 2013, when rainfall amount was 20.4 mm. As shown, the pore-water pressure increment was sharp and equal to 149.5 kPa. Also, the depth of rainfall infiltration was only in the slope surface of red clay. As weathered gneiss rock was less affected by rainfall infiltration, the water content distribution of the slope was in line with pore-water pressure; the water content at the top of the slope was less than that at the bottom of the slope and at surface of the slope was less than at the inner of the slope.

The simulated distributions of the various characteristics of slope of the pore-water pressure, pore-water pressure increment, and water content on August 4, 2013, are shown in Figure 9. Figure 9(a) shows the pore-water pressure distribution under rainfall of 58.8 mm. At this stage, the pore-water pressures of the entire red clay soil domain varied from -535 kPa to 166 kPa. Rainfall of 58.8 mm was more than saturation permeability coefficient of 1.69×10^{-7} m/s. As shown in Figure 8(b), the pore-water pressure of the slope increased along surface, which had a significant impact on red clay.

Figure 10 demonstrates the variation characteristics of slope of the pore-water pressure, pore-water pressure increment, and water content on August 9, 2013. Rainfall was 10 mm on August 5, 2013, which was less than the infiltration rate; rainfall made full infiltration into the surface of the slope of red clay and the pore-water pressure of red clay decreased by rainfall infiltration. Rainfall was 21.5 mm on August 9, 2013; the pore-water pressures in the entire red clay and weathered gneiss rock domain varied from −428.9 kPa to 166.7 kPa. The pore-water pressure decreased and rainfall infiltration range of the slope increased. Maximum infiltration depth was 30 m under surface of the slope.

The effects of the pore-water pressure, pore-water pressure increment, and water content by rainfall are illustrated in Figures 11 and 12. Rainfall was 81 mm and 22 mm on August 13 and August 14, 2013, respectively, which was more than the infiltration rate of the slope. It is clear from Figures 11 and 12 that the maximum pore-water pressures were 413 kPa and 390 kPa, and the maximum pore-water pressure increments were 312.4 kPa and 318 kPa for the slope on August 13 and August 14, 2013, respectively. Maximum infiltration depth occurred in strong weathered gneiss rock under surface of the slope.

Rainfall infiltration amount is related to the permeability coefficient of soil and the permeability coefficient of unsaturated soil depends on the soil water content; the processes of supplementing, runoff, and draining of rainfall; and the change of soil water content. Water content of soil changes the saturation

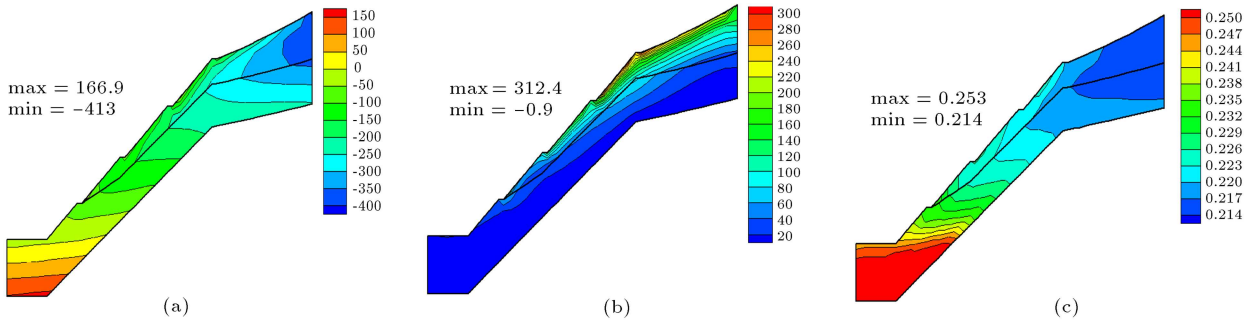

Figure 11. Simulated results at the study site: (a) Pore-water pressure (kPa) on August 13, 2013, (b) the increment of pore-water pressure (kPa) on August 13, 2013, and (c) water content on August 13, 2013.

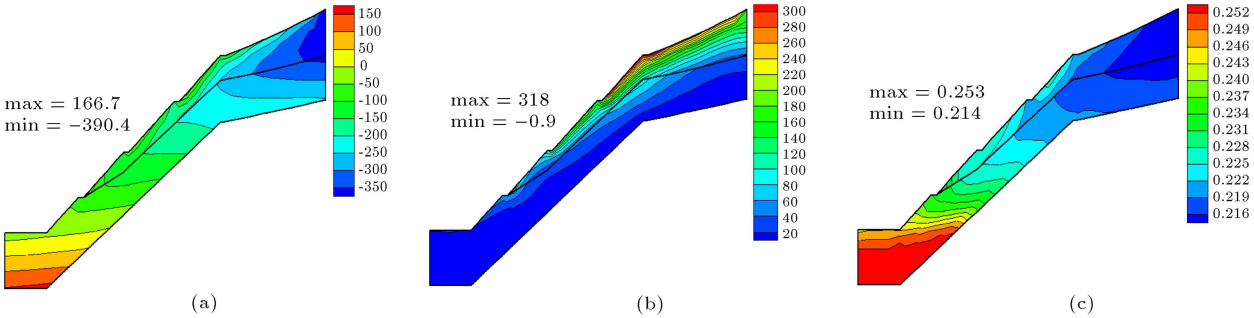

Figure 12. Simulated results at the study site: (a) Pore-water pressure (kPa) on August 14, 2013, (b) the increment of pore-water pressure (kPa) on August 14, 2013, and (c) water content on August 14, 2013.

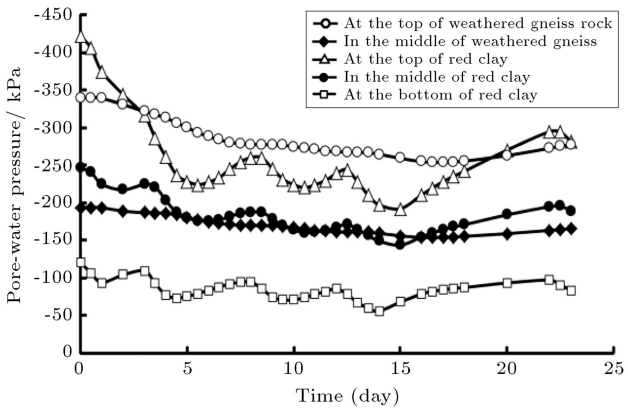

Figure 13. Pore-water pressure curves for monitoring stations of the slope.

state, which causes the matrix suction to gradually lose its function. In order to analyze the seepage characteristics of rainfall, pore-water pressure monitoring stations were set up at the top, middle, and bottom of the slope, respectively. The changes of pore-water pressure monitoring stations of the slope are illustrated in Figure 13. Pore-water pressures were greatly affected by rainfall, more at the top of the slope than at in the middle and bottom of the slope. It is also illustrated that the saturated zone was gradually spread down from the top of the slope. Pore-water pressures increased in red clay before August 6, 2013, and underwent significant changes in the middle and bottom of red clay after August 9, 2013, because the thickness of the clay decreased from top to bottom of the slope. Pore-water pressures were not significantly affected in weathered gneiss rock from August 1 to August 23, 2013, because the changes were mainly due to rainfall infiltration into the red clay layer, and the influence of rainfall on weathered gneiss rock with hysteresis characteristics. During the process of rainfall infiltration, the infiltration boundary is determined by the relationship between rainfall intensity and infiltration capacity. When the rainfall intensity is less than the infiltration capacity, the surface of red soil is in an unsaturated state. On the other hand, when the rainfall intensity is greater than the infiltration capacity, red clay reaches saturated state and red clay infiltration process is gradually reduced. On August 17, 2013, slope failure occurred.

4.2. Influence of the Factor Of Safety (FOS)

The resulting variation in the Factor Of Safety (FOS) of the slope is shown Figure 14. Initially, on August 1, 2013, the FOS was 1.2; then, it had decreasing trend with rainfall increasing and reaching 234 mm during 23 days. The FOS of the slope obviously decreased before August 14, because rainfall failed to infiltrate into weathered gneiss rock. As shown, the predicted FOS successfully simulates timing of the actual failure

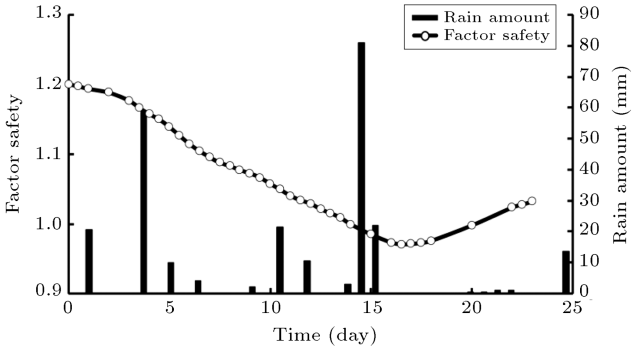

Figure 14. Safety factor versus time.

event. The Factor Of Safety (FOS) of the slope reached the minimum value of 0.97 on August 17, at which the failure occurred.

5. Discussion and conclusion

This paper presents a case study of the failure of an engineering slope due to rainfall in China. A detailed numerical modeling was carried out to simulate the distributions of pore-water pressure, the increment of pore-water pressure, water content, and safety factor for an actual slope in Yunnan. The following conclusions can be drawn from the study:

1. An unsteady saturated-unsaturated seepage mathematical model was described, through the analysis of the stability and seepage under antecedent rainfall conditions of the slope, to understand the law of infiltration by rainfall. The simulated results showed that antecedent rainfall had a significant effect on the slope stability. Rainfall infiltration process, based on the unsteady saturated-unsaturated seepage mathematical model, could reasonably explain the time lag between the occurrence of rainfall and landslides;
2. It was shown that pore-water pressure significantly changed at the top of red clay slope, which was liable to produce large collapsing deformation. The cracks at the top of the slope agreed with the observation before landslide;
3. The suction of soil in the whole weathering gneiss was obviously lagging behind the change of the external atmospheric environment. The suction of the soil layer in the whole weathering gneiss was slowly decreasing under the infiltration of the upper rain, which also happened in the heavy rain after the end of the period of the season;
4. The decrease in amplitude of the suction was more intense on the top of red clay than in the middle and the front edge of the slope, and the thickness of red clay on the top of the slope was more than that in the middle and front of the slope. The saturated zone of landslide gradually expanded from the top to the bottom of the slope;
5. The infiltration process based on saturated-unsaturated Richards equation could reasonably explain the time lag of landslide. The major reason for landslide was that the stagnant water on the surface after rainfall gradually infiltrated into the weathered gneiss rock, resulting in the decrease in the strength of weathered gneiss rock, and then the weight of later rainfall caused the landslide of the slope. The landslide was shallow, induced by antecedent rainfall;
6. From the numerical analysis results, it was found that the factor of safety was 1.2 on August 1, 2013, and, although fluctuating, it followed a decreasing trend. The FOS of the slope decreased slowly before August 14, because rainfall failed to infiltrate into weathered gneiss rock. The FOS reduced to a minimum of 0.97 on August 17, when the failure occurred.

Acknowledgments

This research was supported by The Fundamental Research Funds of the Central Public Welfare Research Institute (Grant No. Y716009, Y716010), and National Natural Science Foundation of China (Grant No. 51609164, 51679151, 41671504, 51779154, JZ2016GJQN0928).

References

1. Basile, A., Mele, G., and Terribile, F. "Soil hydraulic behavior of a selected benchmark soil involved in the landslide of Sarno 1998", *Geoderma.*, **117**(34), pp. 331-336 (2003).
2. Ost, L., Van, J., Poesen, J., et al. "Characteristics and spatial distribution of large landslides in the Flemish Ardennes (Belgium)", *Zeitschrift gur Geomorphologie*, **47**(3), pp. 329-350 (2003).
3. Li, Y.J., Hicks, M.A., and Nuttall, J.D. "Comparative analyses of slope reliability in 3D", *Engineering Geology*, **196**, pp. 12-23 (2015).
4. Brand, E. "Landslide in southeast Asia: A state of the art report", *4th Int. Conf. on Landslides.*, Toronto, Canada (1984).
5. Lim, T.T., Rahardjo, H., Chang. M.F., and Fredlund D.G. "Effect of rainfall on matric suctions in a residual soil slope", *Can. Geotech. J.*, **33**, pp. 618-628 (1996).
6. Rahardjo, H., Li, X.W., and Toll, D.,G. "The effect of antecedent rainfall on slope stability", *Geotechnical and Geological Engineering*, **19**, pp. 371-399 (2001).
7. Lumb, P. "Slope failures in Hong Kong", *Quarterly Journal of Engineering Geology*, **8**, pp. 31-65 (1975).
8. Au, S.W.C. "Rain-induced slope instability in Hong Kong", *Engineering Geology*, **51**(1), pp. 1-36 (1998).

9. Brand, E.W., Premchitt, J., and Phillipson, H.B. "Relationship between rainfall and landslides in Hong Kong", *4th Int. Conf. on Landslides*, Toronto, Canada, pp. 377-384 (1984).

10. Tan, S.B., Tan, S.L., Lim, T.L., and Yang, K.S. "Landslide problems and their control in Singapore", *9th Southeast Asian Geotechnical Conference*, Bankok, Thailand (1987).

11. Wei, J., Heng, Y.S., Chow, W.C., and Chong, M.K. "Landslide at Bukit Batok sports complex", *9th Asian Conference on Soil Mechanics and Foundation Engineering*, Bankok, Thailand (1991).

12. Rahardio, H. and Leong, E.C. "Response of a residual soil slope to rainfall", *Canadian Geotechnical Journal*, **42**(2), pp. 340-351 (2005).

13. Lu, N. and Godt, J.W. "Infinite slope stability under unsaturated seepage conditions", *Water Resour Research*, **44**, pp. 104-114 (2008).

14. Lu, N. and Godt, J.W., *Hillslope Hydrology and Stability*, Cambridge, U.K (2013).

15. Lu, N. and Kaya, M. "A drying cake method for measuring suction stress characteristic curve, soil-water retention and hydraulic conductivity function", *Geotech. Test. J.*, **36**, pp. 1-9 (2013).

16. Campbell, R.H. and Slips, S. "Debris flows and rainstorms in the Santa Monica mountains and vicinity, Southern California", *Geological Survey Professional Paper*, p. 51 (2013).

17. Montgomery, D.R. and Dietrich, W.E. "A physically based model for the topographic control on shallow landsliding", *Water Resource Research*, **30**(4), pp. 1153-1171 (1994).

18. Montrasio, L. and Valetino, R. "A model for triggering mechanisms of shallow lanslides", *Natural Hazards Earth System Science*, **8**, pp. 1149-1159 (2008).

19. Bordoni, M., Meisina, C., Valentin, R., Lu., N., et al. "Hydrological factors affecting rainfall-induced shallow landslides: From the field monitoring to a simplified slope stability analysis", *Engineering Geology*, **193**, pp. 19-37 (2015).

20. Vanapalli, S.K., Fredlund, D.G., Pufahl, D.E., et al. "Model for the prediction of shear strength with respect to soil suction", *Can. Geotech. J.*, **33**, pp. 379-392 (1996).

21. Godt, J.W., Baum, R.L., Savage, W.Z., et al. "Transient deterministic shallow landslide modelling: requirements for susceptibility and hazard assessment in a GIS framework", *Engineering Geology*, **102**, pp. 214-226 (2008a).

22. Godt, J.W., Schulz, W.H., and Baum, R.L. "Modelling rainfall conditions for shallow landsliding in Seattle, Washington. *Landsliding and Engineering Geology of the Seattle Washington Area*, In: Baum, R.L, Dodt, J.W., and High, L.M. (Eds.), *Engineering Geology*, **20**, pp. 137-152 (2008b).

23. Godt, J.W., Baum, R.L., and Lu, N. "Landsliding in partially saturated materials", *Geophys. Res. Lett.*, **36**, pp. 23-29 (2009).

24. Ng, C.W.W. and Shi, Q. "A numerical investigation of the stability of unsaturated soil slopes subjected to transient seepage", *Computers and Geotechnics*, **22**(1), pp. 1-28 (1998).

25. Tsaparas, I., Rahardjo, H., Toll, D.G., and Leong, E.C. "Controlling parameters for rainfall induced landslides", *Computers and Geotechnics*, **29**, pp. 1-27 (2002).

26. Bishop, A.W. "The use of pore-pressure coefficients in practice", *Geotechnique*, **20**(2), pp. 148-152 (1954).

27. Morgenstern, N.R. and Price, V.E. "The analysis of the stability of general slip surface", *Geotechnique*, **15**(4), pp. 289-290 (1965).

28. Spencer, E. "A method of analysis of embankments assuming parallel interslice forces", *Geotechnique*, **17**(1), pp. 11-26 (1967).

29. Ducan, J.M. "State of the art: Limit equilibrium and finite element analysis of slopes", *J. Geotech. Geoenviron*, **122**(7), pp. 577-596 (1996).

30. Borja, R.I. and White. J.A. "Continuum deformation and stability analyses of a steep hillslide slope under rainfall infiltration", *Acta Geotech.*, **5**, pp. 1-4 (2010).

31. Buscarnera, G. and Whittle. A. "Constitutive modelling approach for evaluating the triggering of flow slides", *Can. Geotech. J.*, **49**(5), pp. 499-511 (2012).

32. Sebong, O. and Ning, L. "Slope stability analysis under unsaturated conditions: Case studies of rainfall-induced failure of cut slopes", *Engineering Geology*, **184**, pp. 96-103 (2015).

33. Fredlund, D.G., Morgensterm, N.R., and Widger, R.A. "The shear strength of unsaturated soil", *Canadian Geotechnical Journal*, **15**(3), pp. 313-321 (1978).

Biographies

Zhuo Li is an Associate Professor in Dam Safety Management Department, Nanjing Hydraulic Research Institute. He received a PhD in Hydraulic Engineering, in 2013. His research interests are in the earth and rockfill dam engineering, and hydraulic structures antifreeze in cold regions. He has published 22 journal articles and 3 books.

Yongjun He is Professor in Dam Safety Management Department, Nanjing Hydraulic Research Institute. He received a PhD in Hydraulic Engineering, in 2007. His research interests are in the earth and rockfill dam engineering.

Hongen Li is a Professor in Dam Safety Management Department, Nanjing Hydraulic Research Institute. He received a PhD in Hydraulic Engineering, in 2010. His research interests are in numerical simulation of rockfill

dam and dam safety management. He has published 18 journal articles and 4 books.

Liujiang Wang is an Associate Professor in the College of Water Conservancy and Hydropower Engineering, Hohai University. He has a PhD in Hydraulic Engineering, received in 2012. His research interests are in the earth and rockfill dam engineering.

Yanqiao Wang is an Associate Professor in the School of Civil Engineering, Hefei University of Technology. She has a PhD in Hydraulic Engineering, received in 2011. Her research interests are in the earth and rockfill dam engineering.